Since January 2020 Elsevier has created a COVID-19 resource centre with free information in English and Mandarin on the novel coronavirus COVID-19. The COVID-19 resource centre is hosted on Elsevier Connect, the company's public news and information website.

Antiviral Research 173 (2020) 104646

Contents lists available at ScienceDirect

Antiviral Research

journal homepage: www.elsevier.com/locate/antiviral

Non-invasive bioluminescence imaging of HCoV-OC43 infection and therapy in the central nervous system of live mice

Junwei Niu[a,1], Liang Shen[b,c,1], Baoying Huang[a], Fei Ye[a], Li Zhao[a], Huijuan Wang[a], Yao Deng[a], Wenjie Tan[a,d,*]

[a] Key Laboratory of Biosafety, National Health Commissions, National Institute for Viral Disease Control and Prevention, China CDC, Beijing, 102206, China
[b] Department of Clinical Laboratory, Xiangyang Central Hospital, Affiliated Hospital of Hubei University of Arts and Science, Hubei Province, Xiangyang, 441021, China
[c] Key Laboratory of Molecular Medicine, Medical College, Hubei University of Arts and Science, Xiangyang, 441053, China
[d] Center for Biosafety Mega-Science, Chinese Academy of Sciences, China

ARTICLE INFO

Keywords:
Coronavirus
Bioluminescence imaging
Mouse
Chloroquine
Therapy

ABSTRACT

Human coronaviruses (HCoVs) are important pathogens that cause upper respiratory tract infections and have neuroinvasive abilities; however, little is known about the dynamic infection process of CoVs *in vivo*, and there are currently no specific antiviral drugs to prevent or treat HCoV infection. Here, we verified the replication ability and pathogenicity of a reporter HCoV-OC43 strain expressing Renilla luciferase (Rluc; rOC43-ns2DelRluc) in mice with different genetic backgrounds (C57BL/6 and BALB/c). Additionally, we monitored the spatial and temporal progression of HCoV-OC43 through the central nervous system (CNS) of live BALB/c mice after intranasal or intracerebral inoculation with rOC43-ns2DelRluc. We found that rOC43-ns2DelRluc was fatal to suckling mice after intranasal inoculation, and that viral titers and Rluc expression were detected in the brains and spinal cords of mice infected with rOC43-ns2DelRluc. Moreover, viral replication was initially observed in the brain by non-invasive bioluminescence imaging before the infection spread to the spinal cord of BALB/c mice, consistent with its tropism in the CNS. Furthermore, the Rluc readout correlated with the HCoV replication ability and protein expression, which allowed quantification of antiviral activity in live mice. Additionally, we validated that chloroquine strongly inhibited rOC43-ns2DelRluc replication *in vivo*. These results provide new insights into the temporal and spatial dissemination of HCoV-OC43 in the CNS, and our methods provide an extremely sensitive platform for evaluating the efficacy of antiviral therapies to treat neuroinvasive HCoVs in live mice.

1. Introduction

Coronaviruses (CoVs) are members of the family *Coronaviridae* in the order *Nidovirales* and the genus *Coronavirus* (Adams et al., 2016). CoVs are enveloped, single-stranded, positive-sense RNA viruses that have the largest genome among RNA viruses (~32 kb) (Perlman and Netland, 2009) and are widespread and naturally infect a variety of species. Currently, six CoVs have been identified that predominantly cause respiratory and central nervous system (CNS) pathologies in humans. HCoV-OC43 and HCoV-229E usually cause common colds during the winter and early spring (Larson et al., 1980), whereas HCoV-NL63 is responsible for causing croup in children and results in more severe clinical features than those of HCoV-OC43 or HCoV-229E (Arden et al., 2005; Fouchier et al., 2004; van der Hoek et al., 2004). HCoV-HKU1 is associated with bronchiolitis and pneumonia (Woo et al., 2005a, 2005b). In 2003, an outbreak of severe acute respiratory syndrome (SARS), a lethal zoonotic CoV infection, was reported in China and associated with SARS-CoV (Ksiazek et al., 2003). In 2012, a SARS-like disease emerged that resulted in a mortality rate of 30%, the causative agent of which was identified as Middle East respiratory syndrome CoV (MERS-CoV) (Gralinski and Baric, 2015; Milne-Price et al., 2014). Despite their status as infectious respiratory pathogens, CoVs can also damage the CNS and cause neurological diseases (Arabi et al., 2015; Arbour et al., 2000; Burks et al., 1980; Hung et al., 2003; Morfopoulou et al., 2016; Netland et al., 2008), with HCoV-OC43, HCoV-229E, and SARS-CoV detected in the cerebrospinal fluid of

* Corresponding author. MHC Key Laboratory of Biosafety, National Institute for Viral Disease Control and Prevention, China CDC; Center for Biosafety Mega-Science, Chinese Academy of Sciences; 155 Changbai Road, ChangPing District, Beijing, 102206, China.
E-mail address: tanwj28@163.com (W. Tan).
[1] Co-first author.

https://doi.org/10.1016/j.antiviral.2019.104646
Received 29 August 2019; Received in revised form 29 October 2019; Accepted 4 November 2019
Available online 06 November 2019

patients with multiple sclerosis (Arbour et al., 2000; Burks et al., 1980; Hung et al., 2003). Recently, severe neurological syndromes were identified as associated with MERS-CoV (Arabi et al., 2015), SASR-CoV reportedly exhibits neuroinvasive properties in the CNS of mice (Netland et al., 2008), and HCoV-OC43 is associated with fatal encephalitis (Morfopoulou et al., 2016). Therefore, CoVs are thought to be responsible for CNS pathologies in a way similar to other known neuroinvasive viruses, such as measles virus, human immunodeficiency virus, and herpes virus (Koyuncu et al., 2013). Until recently, little was known about the process and dynamics of HCoV infection in the CNS, and no effective drugs are currently available for treating patients with these infections; therefore, easily observable animal models are required to understand viral replication and investigate potential therapeutic strategies.

Conventional assays that examine host–pathogen interactions are indispensable for demonstrating the processes of pathogen infection and dissemination. Mouse models are commonly used to study viral replication and dissemination and test potential antiviral drugs; however, this conventional approach has various limitations. The experimental animals must be anatomised at multiple time points to study the sites of infection and quantify pathogen titer, thus requiring a large number of animals. Moreover, these approaches cannot monitor the real-time spatial and temporal progression of infection in the same animal. Bioluminescence imaging (BLI) is a powerful optical technique for the molecular imaging of infectious diseases and therapies. *In vivo* BLI techniques have emerged as powerful complements to conventional assays used for studying pathogen replication and dissemination (Hutchens and Luker, 2007; Luker and Luker, 2008). Renilla luciferase (Rluc), among the most widely distributed and commonly used luciferase enzymes for *in vivo* imaging, is purified from the marine organism *Renilla reniformis* (sea pansy), which exhibits blue-green bioluminescence when catalysis is stimulated. Rluc is ATP-independent and oxidizes coelenterazine to generate bioluminescence (Lorenz et al., 1996). Upon oxidation by Rluc *in vitro*, coelenterazine produces blue light with a peak emission at ~480 nm (Matthews et al., 1977). Unlike other luciferases, Rluc has smaller components, high specificity and sensitivity, and can be genetically fused with other proteins, which is particularly useful when investigating pathogens with large genome restrictions (Venisnik et al., 2007).

Non-invasive imaging methods that can monitor viral replication in living animals are more convenient for the temporal and spatial investigation of viral dissemination and pathogenesis than conventional assays. Moreover, the same living animal can be monitored at different time points, thereby reducing the number of animals required to generate sufficient data. The use of recombinant viruses tagged with luciferase is less well studied but becoming increasingly popular. Previously, we used a recombinant Rluc-expressing virus based on the HCoV-OC43 backbone (rOC43-ns2DelRluc) to screen anti-CoV agents and antiviral host factors (Shen et al., 2016). HCoV-OC43 belongs to the genus *Betacoronavirus* along with severe SARS-CoV and MERS-CoV (McIntosh et al., 1967; St-Jean et al., 2004) and in which important replication-related genes are conserved, including *3Clpro*, *RdRp*, and *RNA helicase* (van Boheemen et al., 2012; Woo et al., 2010). HCoV-OC43 causes only mild infection in humans but can cause severe CNS pathology in suckling mice and be manipulated in biosafety level 2 facilities. Moreover, rOC43-ns2DelRluc shows robust growth kinetics and identical virulence to the wild-type virus *in vivo*.

Chloroquine (CQ), a 4-aminoquinoline approved by the Food and Drug Administration to treat malaria, has long been prescribed prophylactically to pregnant women at risk of exposure to *Plasmodium* parasites (Levy et al., 1991). CQ reportedly exhibits antimalarial, anti-inflammatory, and antiviral activities, with *in vitro* efficacy against several viruses, including CoVs (Wilde De et al., 2014); however, real-time data concerning its *in vivo* distribution during viral infection and anti-CoV activity in living animals remains limited.

Here, we utilized rOC43-ns2DelRluc to study the timing of HCoV replication and dissemination in the CNS of mice and verified CQ as a CoV inhibitor *in vivo* by using non-invasive BLI in living mice. Our study provides new insights into CoV replication and dissemination in the CNS and offers a convenient and valuable method for identifying anti-HCoV drugs capable of treating neurological symptoms.

2. Materials and methods

2.1. Cells and antibodies

BHK-21 cells were grown in Dulbecco's modified Eagle medium (Gibco, Gaithersburg, MD, USA) supplemented with 10% fetal bovine serum (Gibco) and 2 mM L-glutamine (Gibco) at 37 °C and 5% CO_2. Anti-β-actin (4970s) rabbit monoclonal antibodies were purchased from Cell Signaling Technology (Danvers, MA, USA). Anti-rabbit (5230–0403) and anti-mouse (5230–0347) IgG (H + L) were purchased from KPL (Gaithersburg, MD, USA). Anti-Rluc (ab185925) rabbit monoclonal and goat anti-rabbit IgG (ab150077) antibodies were purchased from Abcam (Cambridge, UK). Anti-OC43-N mouse polyclonal antibodies were prepared in our laboratory, and goat anti-mouse IgG (A28175) secondary antibodies were purchased from Life Technologies (Carlsbad, CA, USA). Anti-NeuN mouse monoclonal (Mab377) antibodies were purchased from Millipore (Billerica, MA, USA), and goat anti-mouse IgG (H + L) (A11031) secondary antibodies were purchased from Life Technologies. Anti-microtubule-associated protein 2 (MAP2; ab5392) chicken polyclonal antibodies and goat anti-chicken (ab150176) polyclonal antibodies were purchased from Abcam.

2.2. Animal experiments

BALB/c and C57BL/6 mice were purchased from the Animal Care Centre, Chinese Academy of Medical Science (Beijing, China). The study protocol was approved by the Committee on the Ethics of Animal Experiments of the Chinese Center for Disease Control and Prevention. Pathogen-free mice were housed and used in accordance with the guidelines of the Chinese Regulations for the Administration of Affairs Concerning Experimental Animals. BALB/c (12-days old) or C57BL/6 (7-days old) mice were intracerebrally or intranasally inoculated with rOC43-ns2DelRluc or HCoV-OC43-wild-type (WT) for subsequent assays.

2.3. Tissue homogenization

Whole brain, spinal cord, spleen, heart and blood were collected from rOC43-ns2DelRluc-infected mice, homogenized in phosphate-buffered saline (PBS) using a FastPrep instrument (MP Biomedical, Strasbourg, France) and centrifuged at 14,000 rpm for 10 min at 4 °C to remove tissue debris. The supernatant was collected and aliquoted for further study.

2.4. Western blot

Brain and spinal homogenates were separated by 12% sodium dodecyl sulfate-polyacrylamide gel electrophoresis and transferred to nitrocellulose membranes, which were blocked with 5% skim milk at room temperature for 2 h and incubated with anti-OC43-N mouse polyclonal or anti-β-actin antibodies at 4 °C overnight. After washing with PBS with Tween-20, the membranes were incubated with anti-mouse IgG (1:10,000; KPL) or anti-rabbit IgG (1:5000; KPL) at room temperature for 1 h. Blots were scanned to detect infrared fluorescence using the Odyssey infrared imaging system (Li-Cor Biosciences, Lincoln, NE, USA).

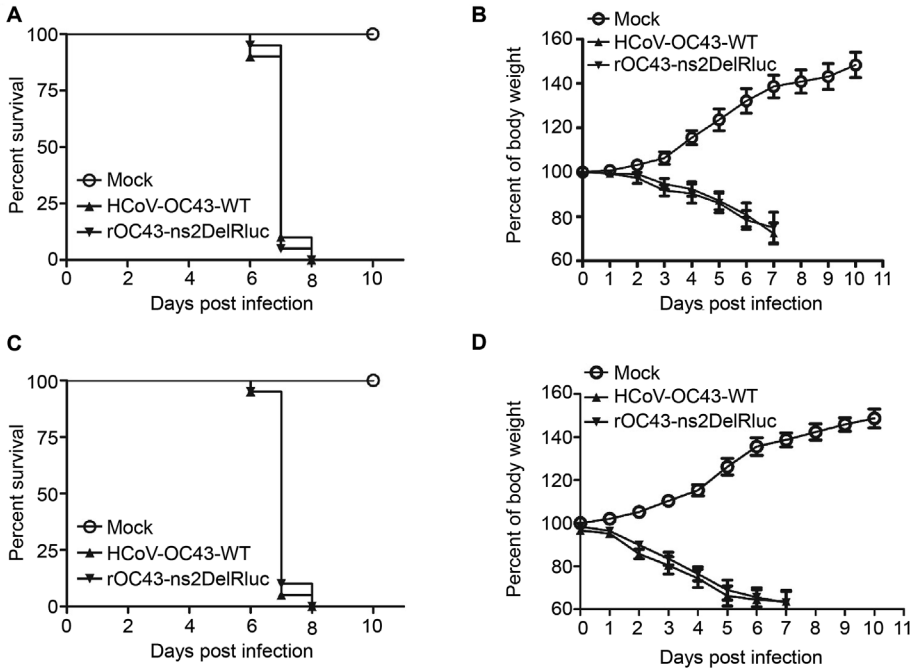

Fig. 1. rOC43-ns2DelRluc is fatal in suckling mice. (A and B) BALB/c mice and (C and D) C57BL/6 mice were intranasally infected with 10^4 $TCID_{50}$ of rOC43-ns2DelRluc (n = 20/group). Weight loss (B and D) and survival (A and C) were monitored daily.

2.5. RNA isolation and quantitative reverse transcription polymerase chain reaction (qRT-PCR)

Total RNA was isolated from the tissue-homogenate supernatants of virus-infected mice using TRIzol reagent (Invitrogen, Carlsbad, CA, USA), and the relative amount of viral genomic rOC43-ns2DelRluc RNA was quantified using qRT-PCR, as described previously (Niu et al., 2016) and the following primers and probe: forward, 5′-GCTCAGGAA GGTCTGCTCC-3′; reverse, 5′-TCCTGCACTAGAGGCTCTGC-3′; and the probe FAM-TTCCAGATCTACTTCGCGCACATCC-TAMRA.

2.6. Viral titration

The rHCoVs-OC43 50% tissue culture infectious dose ($TCID_{50}$) was determined by indirect immunofluorescence assay (IFA) according to a previously described method (Reed, 1938). Briefly, BHK-21 cells in 96-well plates were inoculated with serial 10-fold dilutions of virus, and virus-infected cells were incubated with anti-OC43-N mouse polyclonal antibodies at 72-h post -infection. Goat anti-mouse IgG (A28175) antibodies were used as the secondary antibody.

2.7. Immunofluorescence assay

The brain and spinal cord dissected from rOC43-ns2DelRluc-infected mice and control mice at 6-days post-infection (dpi) were fixed in 10% neutral-buffered formalin, embedded in paraffin, and routinely sectioned to a thickness of ~5 μm. The sections were then permeabilized with 0.3% Triton X-100 in PBS for 30 min, blocked with 5% bovine serum albumin for 1 h at room temperature, and incubated with primary antibodies, including anti-Rluc rabbit monoclonal antibodies, anti-NeuN antibodies and anti-MAP2 antibodies, at 4 °C overnight. Sections were then incubated with secondary antibodies, including Alexa Fluor 488-conjugated goat anti-rabbit (ab150077), Alexa Fluor 568-conjugated goat anti-mouse IgG (H + L) and Alexa Fluor 596-conjugated goat anti-chicken polyclonal antibodies at 37 °C for 1 h. After staining with 1 μg/mL 4′,6-diamidino-2-phenylindole (Sigma-Aldrich, St. Louis, MO, USA) for 30 min, the sections were covered with Permount, and images were captured by Operetta (PerkinElmer, Waltham, MA, USA) with Columbus software or by a Leica TCS SP8 confocal microscope with LAS software (Leica Biosystems, Wetzlar, Germany).

2.8. BLI analysis

rOC43-ns2DelRluc replication in mice was evaluated by BLI with an In Vivo F Pro (Bruker Daltonik, Bremen, Germany). Prior to imaging, rOC43-ns2DelRluc-infected mice were injected intraperitoneally with Renilla luciferase substrate (20 μg/g; Promega, Madison, WI, USA) and anaesthetized with isoflurane. After 5 min, mice were placed on a light-tight camera box stage under continuous anesthesia, imaged (acquisition time: 4 min), and the signals were quantified using Bruker molecular imaging software (Bruker).

2.9. Statistical analysis

All graphs were produced using Prism 5.0 software (GraphPad Software, San Diego, CA, USA), and results are expressed as the mean ± standard error of the mean. Statistical analysis were performed using SPSS (v.21.0; IBM Corp., Armonk NY, USA). Differences were considered statistically significant at $P < 0.05$.

3. Results

3.1. Intranasal rOC43-ns2DelRluc inoculation is fatal to suckling mice

Previously, we constructed several recombinant Rluc-expressing HCoV-OC43-reporter viruses. One reporter virus (rOC43-ns2DelRluc) in which the *ns2* gene was replaced by Rluc showed robust growth kinetics similar to those of HCoV-OC43-WT and high stability after multiple passages *in vitro*. Additionally, rOC43-ns2DelRluc (100 $TCID_{50}$) showed pathogenicity in BALB/c mice, which exhibited neurological symptoms identical to those caused by the parental virus after intracerebral inoculation (Shen et al., 2016).

Viral replication *in vivo* depends on the genetic backgrounds of both the virus and its host. Previous studies reported that inbred BALB/c and C57BL6 mice are susceptible to HCoV-OC43 infection (Jacomy et al.,

2006; Jacomy and Talbot, 2003; Noah et al., 2006). Therefore, these two mouse strains were infected with 10^4 $TCID_{50}$ of rOC43-ns2DelRluc or HCoV-OC43-WT by intranasal inoculation in order to determine its infection of the respiratory tract *in vivo*. As expected, both strains presented typical symptoms of advanced disease (twitching limbs and humped back) after inoculation with rOC43-ns2DelRluc or HCoV-OC43-WT. Intranasal rOC43-ns2DelRluc inoculation led to 100% mortality in both strains, with most mice dying at 7 dpi, similar to those infected with HCoV-OC43-WT (Fig. 1A and C). Additionally, both mouse strains infected with rOC43-ns2DelRluc showed reduced body weight, similar to those infected with HCoV-OC43-WT (Fig. 1B and D). According to a previous report (Jacomy and Talbot, 2003), C57BL/6 mice, especially those > 15-days old, are more sensitive to HCoV-OC43 than BALB/c. However, in the present study, we found that both BALB/c or C57BL/6 suckling mice (< 12-days old) infected with HCoV-OC43 at a dose of 10^4 $TCID_{50}$ showed 100% mortality and similar sensitivity. These results showed that rOC43-ns2DelRluc infection resulted in severe encephalitis and neurological symptoms in both mouse strains, suggesting that rOC43-ns2DelRluc can be used as an infection model for simulating HCoV-OC43-WT CNS infection *in vivo*.

3.2. rOC43-ns2DelRluc replication and dissemination in mice with different genetic backgrounds

To confirm these observations and the dissemination of the recombinant virus, the viral load in different tissues was determined using an IFA in BHK-21 cells or real-time qRT-PCR at 6 dpi via intranasal inoculation of 10^4 $TCID_{50}$ of rOC43-ns2DelRluc. In line with the symptoms, we detected high viral titers in the brains and spinal cords of both mouse strains (Fig. 2A, upper), whereas low viral RNA levels were detected in the hearts and spleen, and extremely low levels were detected in the blood (Fig. 2A, lower), consistent with previous reports on HCoV-OC43-WT (Dubé et al., 2018; Jacomy and Talbot, 2003). Immunostaining of brain and spinal cord sections from mice that underwent intracerebral infection confirmed the presence of rOC43-ns2DelRluc (Fig. 2B), with Rluc detected in neuron cells labeled with MAP2 or NeuN in several areas of the CNS in both mouse strains (Fig. 2C and D). These results suggested rOC43-ns2DelRluc as a promising candidate for BLI in both mouse strains.

3.3. BLI of rOC43-ns2DelRluc-infected mice

To perform BLI of rOC43-ns2DelRluc *in vivo*, BALB/c and C57BL/6 mice were intranasally inoculated with 10^4 $TCID_{50}$ of rOC43-ns2DelRluc or HCoV-OC43-WT, monitored over time, and bioluminescence intensity was determined (Fig. 3). At 6 dpi, signals were observed in the brain and spinal cord when the dorsal side of BALB/c mice was imaged (Fig. 3A), whereas no signals were detected in mice infected with HCoV-OC43-WT (data not shown). Moreover, when the ventral side of BALB/c mice was imaged, no replication was observed (Fig. 3A and B). Surprisingly, no signals were detected in the brains of C57BL/6 mice until their death at 7 dpi; however, by this point we had removed their fur, which might have affected photon transmission from both the dorsal and ventral sides (Fig. 3A and B). Because we confirmed rOC43-ns2DelRluc replication in various mice from both strains, the lack of signals in C57BL/6 mice could have been due to the low penetration and bioavailability of the Rluc substrate in the mice rather than a low viral titer in the CNS. These results indicted that BLI was readily visualized and could be used to quantify rOC43-ns2DelRluc replication and dissemination in the CNS of living BALB/c mice, suggesting this virus as a potential candidate for real-time imaging following inoculation.

3.4. Real-time imaging of rOC43-ns2DelRluc in mice

We then used BLI to study the time course of rOC43-ns2DelRluc replication and dissemination. Briefly, individual BALB/c mice were either inoculated intracerebrally with 100 $TCID_{50}$ or intranasally with 10^4 $TCID_{50}$ of rOC43-ns2DelRluc and monitored over time. Two days after intracerebral inoculation, signals were apparent in the brain from the dorsal side of the mice (Fig. 4A and S1), and at 4 dpi, the signals detected in the brain became more dispersed, and additional signals were detected in the spine (Fig. 4A and S1). Simultaneously, infected BALB/c mice exhibited severe symptoms typical of advanced disease (twitching limbs) and died soon thereafter. Following intranasal inoculation, signals emanating from the brain were observed at 3 dpi and peaked at 7 dpi, whereas signals emanating from the spinal cord were detected at 6 dpi (Fig. 4F and S1), and the mice died at 7 dpi. To verify whether there was a direct correlation between intensity and viral titer, BALB/c mice intracerebrally or intranasally inoculated with rOC43-ns2DelRluc were sacrificed at different time points. Viral replication determined by indirect IFA in the brains and spinal cords revealed a good correlation between relative viral load and bioluminescence intensity (Fig. 4B, D, G, and I), with a high level of correlation between the two variables (Fig. 4C, E, H, and J), particularly in the intracerebral-infection group (Fig. 4C). This result confirmed the efficacy of BLI for assessing viral load in rOC43-ns2DelRluc-infected mice. Western blot analysis (Fig. 4K and L) further validated the time course of rOC43-ns2DelRluc replication in the brain and spinal cord. These findings indicated that BLI revealed the temporal and spatial progression of HCoV-OC43 replication in live mice and provided a non-invasive method for sensitively quantifying small differences.

3.5. Real-time imaging of antiviral agents in vivo

To verify whether BLI of rOC43-ns2DelRluc-infected mice could be used to test the efficiency of antiviral drugs *in vivo*, CQ was administered to mice 2 h before viral inoculation (day 0; 30 mg/kg) and then administered daily according to a previous study of HCoV-OC43-WT (Keyaerts et al., 2009). Mice were intracerebrally infected with 100 $TCID_{50}$ of rOC43-ns2DelRluc, and bioluminescence intensity was measured daily (Fig. 5). No signals were detected in mice treated with CQ, and all of them survived (Fig. 5A, lower), whereas all mice receiving PBS displayed increased bioluminescence and died (Fig. 5A; upper), demonstrating a significant difference relative to the individual controls (Fig. 5B and C). Western blot analysis confirmed the difference in rOC43-ns2DelRluc replication between mice treated with or without CQ (Fig. 5D and E). These results showed that rOC43-ns2DelRluc-infected mice could be used as a sensitive *in vivo* tool for testing the efficiency of antiviral drugs against HCoV-OC43 and compounds against a broad-spectrum of CoVs, particularly severe SARS-CoV and MERS-CoV.

4. Discussion

CoVs, which cause respiratory diseases, have also been associated with neurological complications (Arabi et al., 2015; Arbour et al., 2000; Burks et al., 1980; Hung et al., 2003; Netland et al., 2008), with HCoV-OC43 even causing fatal encephalitis (Jacomy et al., 2006; Jacomy and Talbot, 2003; Morfopoulou et al., 2016); however, the mechanisms responsible for their dissemination and penetration in the host CNS remain unclear. Therefore, easily observable, living animal models are required to identify the mechanisms of HCoV infection in the CNS and enable the development of antiviral drugs for treating and preventing CoV infection and their associated severe CNS pathologies. Here, we used BLI to monitor HCoV-OC43 infection in real-time using the rOC43-ns2DelRluc reporter protein as a direct correlate of viral titer. We confirmed our previous observation by demonstrating that rOC43-ns2DelRluc possesses critical neurotropic and neuroinvasive properties after infection via the respiratory tract. Rluc, which is smaller than Firefly luciferase (Fluc), is useful for producing genetic fusions with other proteins, particularly for viruses with large genomes, such as like

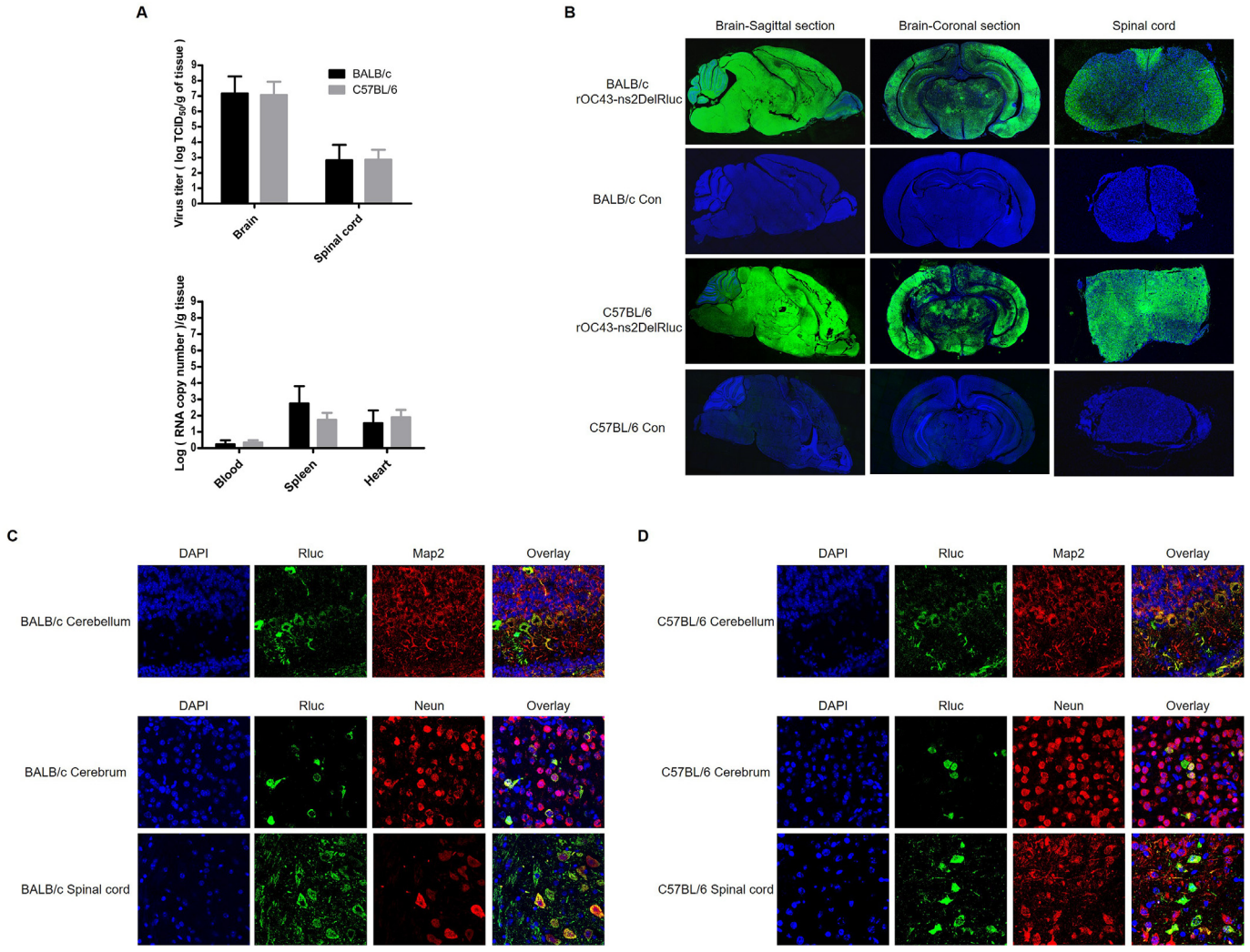

Fig. 2. Replication and dissemination of rOC43-ns2DelRluc in mice with different genetic backgrounds. (A) Detection of rOC43-ns2DelRluc in different tissues. Mice were inoculated intranasally with 10^4 $TCID_{50}$ rOC43-ns2DelRluc and sacrificed at 6 dpi. Tissue supernatants were analyzed for viral load by IFA (upper) in BHK-21 cells or real-time qRT-PCR (lower). Data represent three independent experiments and are shown as the mean ± standard deviation. (B) Immunofluorescence staining of infected and mock-infected mouse brains and spinal cords. (C and D) Double-staining for Rluc and neuron cells in brain and spinal cord sections. Mice were inoculated intranasally with 10^4 $TCID_{50}$ rOC43-ns2DelRluc and sacrificed at 6 dpi. Brain and spinal cord tissues were analyzed using Operetta (PerkinElmer) with Columbus software (B) or a Leica TCS SP8 confocal microscope with LAS software (C and D). Representative graphs are shown of various brain and spinal cord sections from rOC43-ns2DelRluc-infected BALB/c and C57BL/6 mice.

CoVs. Replacing *ns2* with Rluc did not impair viral-replication kinetics, and we observed robust Rluc activity. Moreover, Rluc expression levels correlated well with viral replication in the infected CNS, revealing the dynamic infection process. Therefore, our results demonstrated that BALB/c mice infected with rOC43-ns2DelRluc could be a promising animal model for testing the efficacy of antiviral drugs to treat

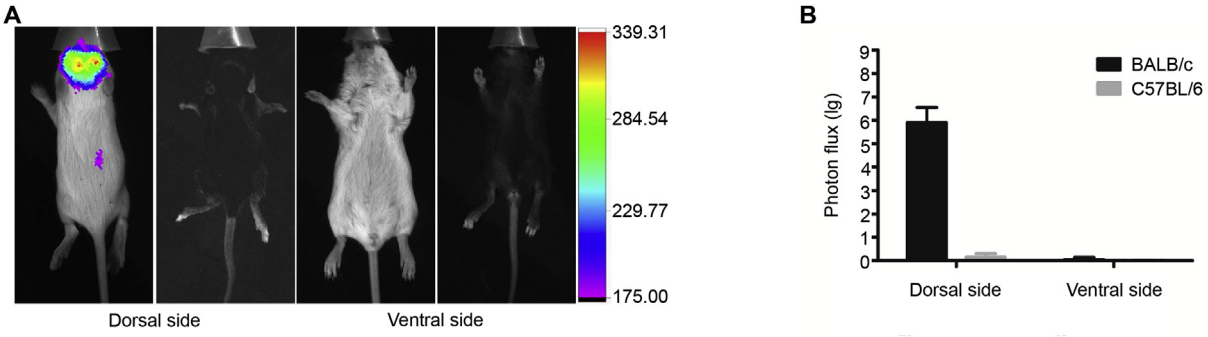

Fig. 3. BLI of rOC43-ns2DelRluc in mice with different genetic backgrounds. (A) BLI of the dorsal and ventral sides of mice with different genetic backgrounds. BALB/c and C57BL/6 mice were intranasally infected with 10^4 $TCID_{50}$ rOC43-ns2DelRluc, and BLI was performed at 6 dpi by intraperitoneal injection of Rluc substrate and capture of photon emission using an In Vivo F Pro system. Representative graphs are shown of the dorsal and ventral views. (B) Comparison of BLI from different sides of mice with different genetic backgrounds. Data represent three independent experiments and are shown as the mean ± standard deviation.

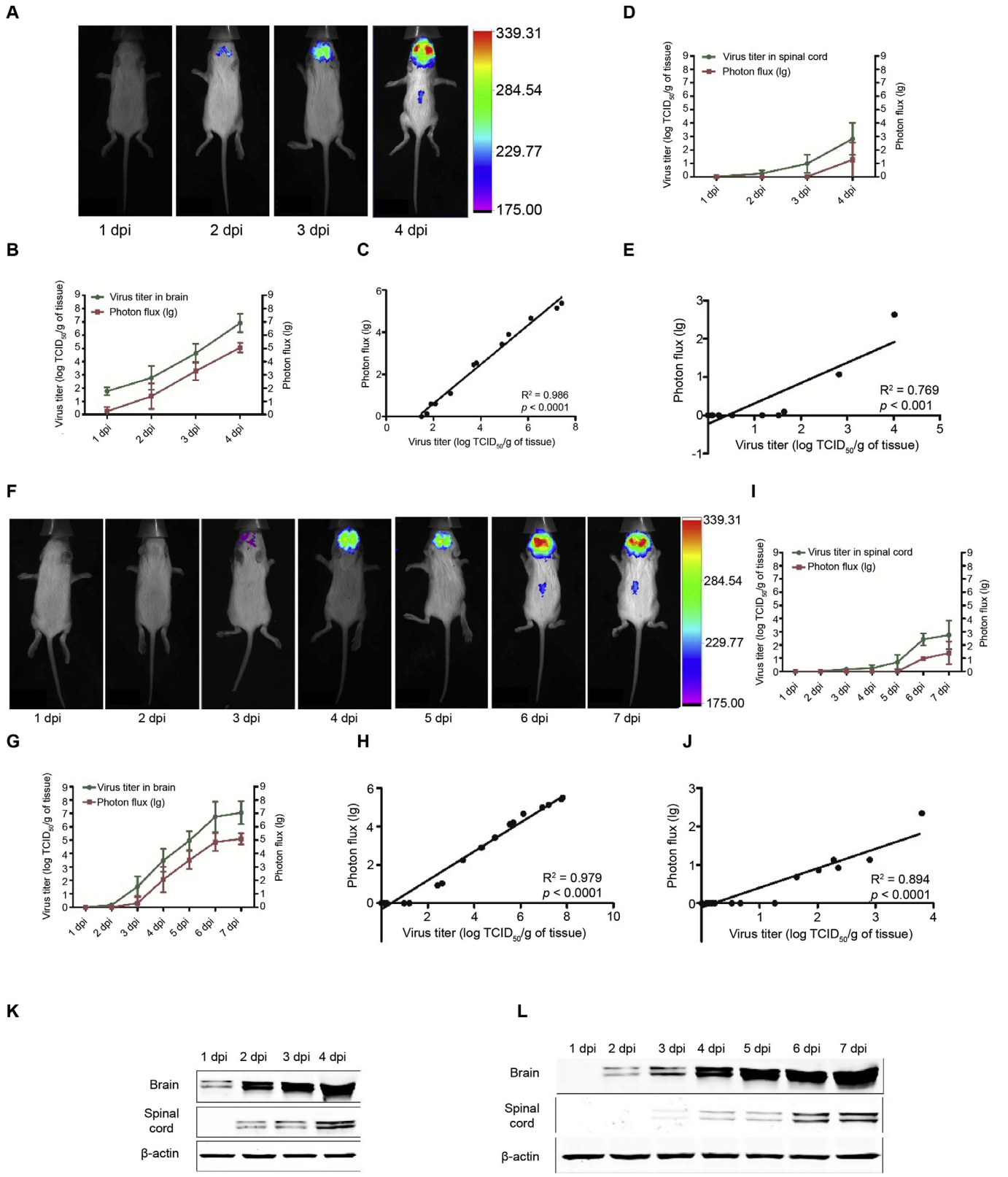

Fig. 4. BLI of the spatial and temporal progression of rOC43-ns2DelRluc infection. BLI of BALB/c mice after intracerebral (A) or intranasal (F) infection with rOC43-ns2DelRluc. BALB/c mice underwent intracerebral (100 $TCID_{50}$) or intranasal (10^4 $TCID_{50}$) inoculation on day 0 with rOC43-ns2DelRluc, and BLI was performed daily by intraperitoneal injection of Rluc substrate and capture of photon emission using an In Vivo F Pro system. Representative BLI images are shown. (B–E) Data correspond to the time course after intracerebral infection. Luciferase activity was quantified using the In Vivo F Pro system, and viral titer was determined by indirect IFA of brain (B) and spinal cord (D) tissue at the indicated time points. The R^2 and *P*-values for the linear regression analysis of brain (C) and spinal cord (E) tissue are indicated on each graph. (G–J) Data correspond to the time course after intranasal infection. Luciferase activity was quantified using the In Vivo F Pro system, and viral titer was determined by indirect IFA of brain (G) and spinal cord (I) tissue at the indicated time points. The R^2 and *P*-values for the linear regression analysis of brain (H) and spinal cord (J) tissue are indicated on each graph. Data represent three independent experiments and are shown as the mean ± standard deviation. Western blot analysis of rOC43-ns2DelRluc replication after intracerebral (K) or intranasal (L) inoculation.

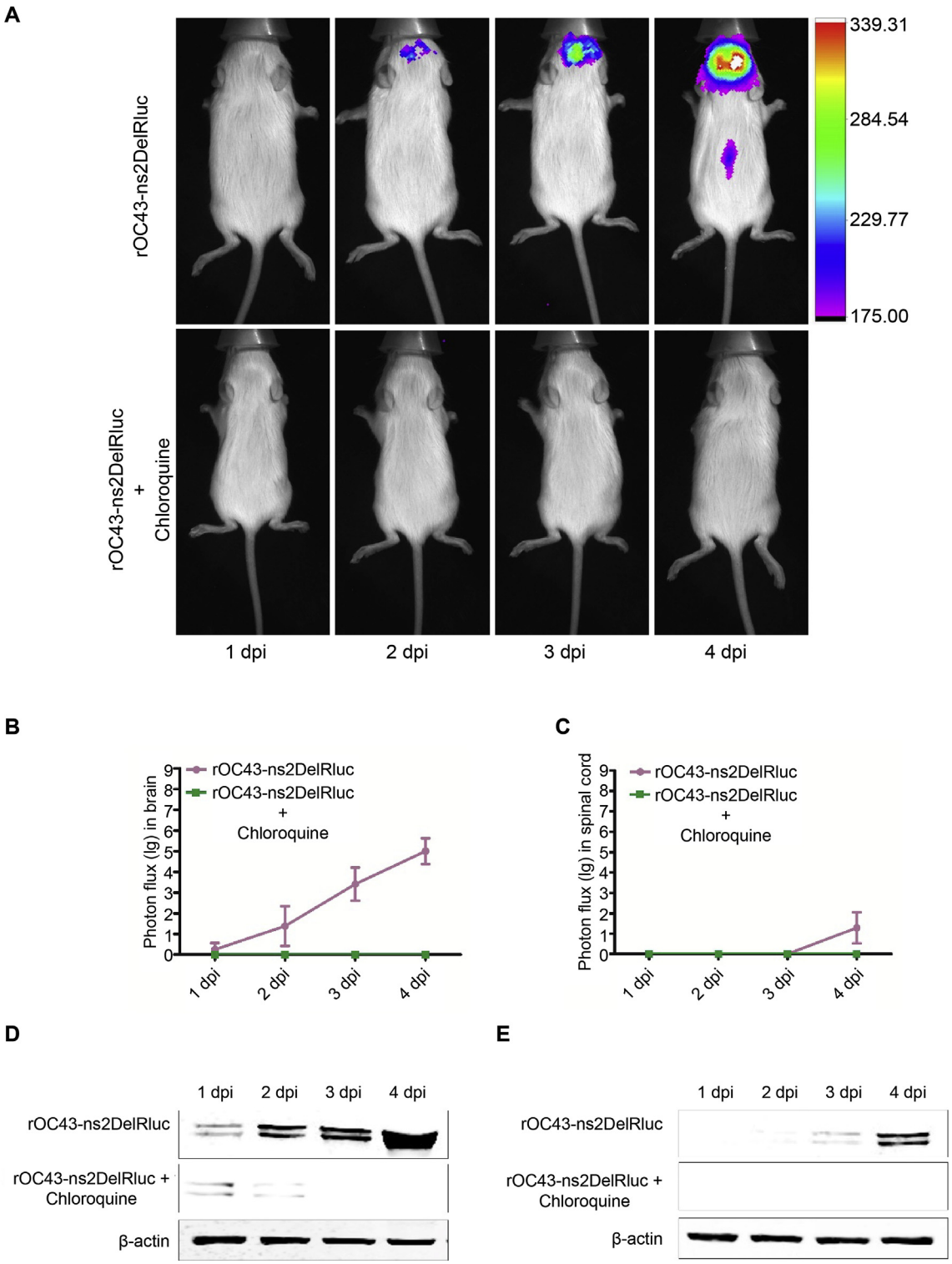

Fig. 5. BLI of rOC43-ns2DelRluc allows evaluation of antiviral therapeutics in living mice. (A) BLI of BALB/c mice treated with or without CQ after rOC43-ns2DelRluc inoculation. Mice infected intracerebrally with 100 $TCID_{50}$ of rOC43-ns2DelRluc were untreated (upper panel) or treated (lower panel) with CQ (30 mg/kg) daily, followed by daily BLI by intraperitoneal injection of Rluc substrate and capture of photon emission using an In Vivo F Pro system. A representative BLI image of one mouse is shown. Comparative time course of BLI of brain (B) and spinal cord (C) tissue of mice treated with or without CQ after rOC43-ns2DelRluc inoculation. Luciferase activity was quantified using an In Vivo F Pro system. Data represent three independent experiments and are shown as the mean ± standard deviation. Western blot analysis of brain (D) and spinal cord (E) tissue from BALB/c mice treated with or without CQ after rOC43-ns2DelRluc inoculation.

neurological symptoms. As expected, CQ, a widely used drug with well-known antimalarial effects, strongly attenuated HCoV-OC43 replication in the brain and prevented the infection from spreading to the spinal cord, consistent with a previous study (Keyaerts et al., 2009).

Acute respiratory syndrome caused by viral infection poses a serious threat to public health due to high morbidity and mortality rates (Tregoning and Schwarze, 2010). Notably, extra-pulmonary symptoms have been described for respiratory viruses such as influenza virus,

human respiratory syncytial virus, and human metapneumovirus, accompanied by neurological complications (Dahm et al., 2016; McGavern and Kang, 2011; Swanson and McGavern, 2015). Different mouse models have been established that are susceptible to these viruses (Cavallaro and Maassab, 1966; Liu et al., 2009; Rameix-Welti et al., 2014; Yu et al., 2014); however, these models do not develop severe CNS pathologies. Li et al. (2017) used BLI to study neurotropic flaviviruses, which can severely damage the central and peripheral nervous systems, showing that viral RNA measured by qRT-PCR directly correlated with Rluc bioluminescence intensity in intracranially inoculated mice. HCoV-OC43, a respiratory CoV, could be a powerful tool for gaining new insights into the neurological manifestations and neurotropic mechanisms of other respiratory viruses. In the present study, our data demonstrated that rOC43-ns2DelRluc levels reflected HCoV-OC43-WT replication in the brain and its spread to the spinal cord of living mice, with bioluminescence intensity directly correlating with viral loads as measured by IFA and western blot and consistent with previous studies (Dubé et al., 2018; Jacomy et al., 2006).

Preclinical animal models that mimic the human pathogenesis of Beta-CoV infection are still urgently needed to develop vaccines and therapies. BLI has emerged as a powerful tool for studying animal models of viral disease, thereby enabling real-time study of viral infection, host immune responses, and the efficacy of intervention strategies *in vivo*. Two animal models using BLI have been reported for studying the relationship between CoVs and their hosts and identifying anti-CoV agents (Fan et al., 2018; Raaben et al., 2009). Raaben et al. (2009) constructed a recombinant virus expressing Fluc based on mouse CoV (MHV-A59) and used it to study viral replication and dissemination *in vivo*; however, MHV-A59 has a complicated tropism in mice. Fan et al. (2018) successfully established a human *dipeptidyl peptidase-4*-knock-in mouse model susceptible to pseudotyped Fluc-expressing MERS-CoV, allowing MERS-CoV to be optically imaged; however, the pseudovirus was unable to replicate, and the authors could only study the entry process. Furthermore, the animal model is not suitable for simulating the pathological CNS symptoms caused by HCoV infection. In the present study, we showed that a BLI-based HCoV-OC43 animal model could be used to test antiviral drug efficacy. CNS luciferase levels accurately represented therapeutic effect, highlighting the potential of the BLI platform to evaluate antiviral drugs for treating HCoV-OC43 infection and its neurological complications by monitoring its replication and dissemination in the same animals in real-time. Although BLI technology is beneficial for studying viral replication and dissemination, it has some inherent limitations. First, hair and organ pigmentation can affect photon transmission; therefore, photon flux from tissues close to the body surface are detected more easily than those from internal organs, with light attenuating at a ~10-fold decrease per cm of tissue (Contag et al., 2010; Contag and Bachmann, 2002). This phenomenon explains why we were only able to detect strong signals from the dorsal rather than the ventral side of infected mice. Second, limited biodistribution, rapid metabolic kinetics, and higher background levels restrict the use of BLI for molecular imaging (Bhaumik and Gambhir, 2002; Pichler et al., 2004; Tannous et al., 2005). Therefore, the genetic background of the host should be taken into account, even if they are permissive to the virus. In the present study, signals were only detected in the CNS of BALB/c mice after inoculation, despite the fact that both C57BL/6 and BALB/c mice are permissive to rOC43-ns2DelRluc. This might be due to the bioavailability of the Rluc substrate, which might not be absorbed and transported to the point of infection with Rluc-expressing viruses (Pichler et al., 2004). This limitation could potentially be overcome by replacing the Rluc reporter in rOC43-ns2DelRluc with Fluc (Contag and Bachmann, 2002; Raaben et al., 2009).

CQ has been tested successfully in several animal models and found to protect 5-day-old suckling mice (survival rate: 100%) following administration at 1-day prepartum to pregnant mice infected with HCoV-OC43 (Keyaerts et al., 2009). Moreover, a survival rate of 70% was observed in BALB/c mice infected with avian influenza H5N1 virus following treatment with 50 mg/kg/day CQ (Yiwu et al., 2013). CQ is widely distributed throughout bodily tissues and fluids, with a higher concentration in the brain than in the plasma. In the present study, *in vivo* data demonstrated that CQ could inhibit HCoV in the CNS of animals. Different mechanisms have been described for the inhibition of viral infection by CQ (Savarino et al., 2003); however, the exact mechanisms by which CQ affects HCoV-OC43 in the CNS of animals requires further study.

In summary, we developed a powerful method for real-time monitoring of HCoV-OC43 replication and dissemination in the CNS. To the best of our knowledge, this is the first report on non-invasive BLI in the CNS of living HCoV-infected mice. Furthermore, rOC43-ns2DelRluc-based BLI is a promising platform for non-invasively screening antiviral compounds *in vivo* and developing new therapeutic strategies. This study will contribute to future studies on CoV-host interactions *in vivo,* the screening of broad-spectrum drugs, and new approaches for studying CNS pathologies caused by respiratory viruses.

Author contributions

J.N., L.S., and W.T. designed the study; J.N., L.S., B.H., F.Y., L.Z., H.W., and Y.D. performed the experiments; J.N., L.S.., B.H., and W.T. analyzed the data; J.N., L.S., and W.T. wrote the paper. All authors reviewed and approved the final manuscript.

Declaration of competing interest

The authors declare no commercial or financial conflicts of interest.

Acknowledgments

We thank Dr. Talbot (INRS-Institute Armand-Frappier, Université du Québec, Laval, Québec, Canada) for providing infectious clone of HCoV-OC43 (WT). This research was funded by the National Key Research and Development Program of China (2016YFD0500301, 2016YFC1200901, and 2018YFC1200602) and the National Major Project for Control and Prevention of Infectious Disease in China (2016ZX10004001-003) from the Ministry of Science and Technology of China and National Health Commissions of China. The funders had no role in study design, data collection and analysis, decision to publish, or preparation of the manuscript. We also thank the staff at the Animal Center affiliated with the Chinese CDC.

Appendix A. Supplementary data

Supplementary data to this article can be found online at https://doi.org/10.1016/j.antiviral.2019.104646.

References

Adams, M.J., Lefkowitz, E.J., King, A.M., Harrach, B., Harrison, R.L., Knowles, N.J., Kropinski, A.M., Krupovic, M., Kuhn, J.H., Mushegian, A.R., Nibert, M., Sabanadzovic, S., Sanfacon, H., Siddell, S.G., Simmonds, P., Varsani, A., Zerbini, F.M., Gorbalenya, A.E., Davison, A.J., 2016. Ratification vote on taxonomic proposals to the international committee on taxonomy of viruses (2016). Arch. Virol. 161, 2921–2949. https://doi.org/10.1007/s00705-016-2977-6.

Arabi, Y.M., Harthi, A., Hussein, J., Bouchama, A., Johani, S., Hajeer, A.H., Saeed, B.T., Wahbi, A., Saedy, A., AlDabbagh, T., Okaili, R., Sadat, M., Balkhy, H., 2015. Severe neurologic syndrome associated with Middle East respiratory syndrome corona virus (MERS-CoV). Infection 43, 495–501. https://doi.org/10.1007/s15010-015-0720-y.

Arbour, N., Day, R., Newcombe, J., Talbot, P.J., 2000. Neuroinvasion by human respiratory coronaviruses. J. Virol. 74, 8913–8921. https://doi.org/10.1128/jvi.74.19.8913-8921.2000.

Arden, K.E., Nissen, M.D., Sloots, T.P., Mackay, I.M., 2005. New human coronavirus, HCoV-NL63, associated with severe lower respiratory tract disease in Australia. J. Med. Virol. 75, 455–462. https://doi.org/10.1002/jmv.20288.

Bhaumik, S., Gambhir, S.S., 2002. Optical imaging of Renilla luciferase reporter gene expression in living mice. Proc. Natl. Acad. Sci. U. S. A. 99, 377–382. https://doi.org/10.1073/pnas.012611099.

Burks, J.S., DeVald, B.L., Jankovsky, L.D., Gerdes, J.C., 1980. Two coronaviruses isolated from central nervous system tissue of two multiple sclerosis patients. Science 80–, 933–934. https://doi.org/10.1126/science.7403860. 209.

Cavallaro, J.J., Maassab, H.F., 1966. Adaptation of respiratory syncytial (RS) virus to brain of suckling mice. Proc. Soc. Exp. Biol. Med. 121, 37–41. https://doi.org/10.3181/00379727-121-30691.

Contag, C.H., Bachmann, M.H., 2002. Advances in in vivo bioluminescence imaging of gene expression. Annu. Rev. Biomed. Eng. 4, 235–260. https://doi.org/10.1146/annurev.bioeng.4.111901.093336.

Contag, C.H., Spilman, S.D., Contag, P.R., Oshiro, M., Eames, B., Dennery, P., Stevenson, D.K., Benaron, D.A., 2010. Visualizing gene expression in living mammals using a bioluminescent reporter. Photochem. Photobiol. 66, 523–531.

Dahm, T., Rudolph, H., Schwerk, C., Schroten, H., Tenenbaum, T., 2016. Neuroinvasion and inflammation in viral central nervous system infections. Mediat. Inflamm. 2016, 8562805. https://doi.org/10.1155/2016/8562805.

Dubé, M., Le, A.C., Wong, A., Rini, J.M., Desforges, M., Talbot, P.J., 2018. Axonal transport enables neuron-to-neuron propagation of HCoV-OC43. J. Virol JVI.00404-18.

Fan, C., Wu, X., Liu, Q., Li, Q., Liu, S., Lu, J., Yang, Y., Cao, Y., Huang, W., Liang, C., Ying, T., Jiang, S., Wang, Y., 2018. A human DPP4-knockin mouse's susceptibility to infection by authentic and pseudotyped MERS-CoV. Viruses 10, 448.

Fouchier, R.A., Hartwig, N.G., Bestebroer, T.M., Niemeyer, B., de Jong, J.C., Simon, J.H., Osterhaus, A.D., 2004. A previously undescribed coronavirus associated with respiratory disease in humans. Proc. Natl. Acad. Sci. U. S. A. 101, 6212–6216. https://doi.org/10.1073/pnas.0400762101.

Gralinski, L.E., Baric, R.S., 2015. Molecular pathology of emerging coronavirus infections. J. Pathol. 235, 185–195. https://doi.org/10.1002/path.4454.

Hung, E.C., Chim, S.S., Chan, P.K., Tong, Y.K., Ng, E.K., Chiu, R.W., Leung, C.B., Sung, J.J., Tam, J.S., Lo, Y.M., 2003. Detection of SARS coronavirus RNA in the cerebrospinal fluid of a patient with severe acute respiratory syndrome. Clin. Chem. 49, 2108–2109. https://doi.org/10.1373/clinchem.2003.025437.

Hutchens, M., Luker, G.D., 2007. Applications of bioluminescence imaging to the study of infectious diseases. Cell Microbiol. 9, 2315–2322. https://doi.org/10.1111/j.1462-5822.2007.00995.x.

Jacomy, H., Fragoso, G., Almazan, G., Mushynski, W.E., Talbot, P.J., 2006. Human coronavirus OC43 infection induces chronic encephalitis leading to disabilities in BALB/C mice. Virology 349, 335–346. https://doi.org/10.1016/j.virol.2006.01.049.

Jacomy, H., Talbot, P.J., 2003. Vacuolating encephalitis in mice infected by human coronavirus OC43. Virology 315, 20–33.

Keyaerts, E., Li, S., Vijgen, L., Rysman, E., Verbeeck, J., Van Ranst, M., Maes, P., 2009. Antiviral activity of chloroquine against human coronavirus OC43 infection in newborn mice. Antimicrob. Agents Chemother. 53, 3416–3421. https://doi.org/10.1128/AAC.01509-08.

Koyuncu, O.O., Hogue, I.B., Enquist, L.W., 2013. Virus infections in the nervous system. Cell Host Microbe 13, 379–393. https://doi.org/10.1016/j.chom.2013.03.010.

Ksiazek, T.G., Erdman, D., Goldsmith, C.S., Zaki, S.R., Peret, T., Emery, S., Tong, S., Urbani, C., Comer, J.A., Lim, W., Rollin, P.E., Dowell, S.F., Ling, A.E., Humphrey, C.D., Shieh, W.J., Guarner, J., Paddock, C.D., Rota, P., Fields, B., DeRisi, J., Yang, J.Y., Cox, N., Hughes, J.M., LeDuc, J.W., Bellini, W.J., Anderson, L.J., Group, S.W., 2003. A novel coronavirus associated with severe acute respiratory syndrome. N. Engl. J. Med. 348, 1953–1966. https://doi.org/10.1056/NEJMoa030781.

Larson, H.E., Reed, S.E., Tyrrell, D.A., 1980. Isolation of rhinoviruses and coronaviruses from 38 colds in adults. J. Med. Virol. 5, 221–229.

Levy, M., Buskila, D., Gladman, D.D., Urowitz, M.B., Koren, G., 1991. Pregnancy outcome following first trimester exposure to chloroquine. Am. J. Perinatol. 8, 174–178.

Li, X.F., Li, X.D., Deng, C.L., Dong, H.L., Zhang, Q.Y., Ye, Q., Ye, H.Q., Huang, X.Y., Deng, Y.Q., Zhang, B., Qin, C.F., 2017. Visualization of a neurotropic flavivirus infection in mouse reveals unique viscerotropism controlled by host type I interferon signaling. Theranostics 7, 912–925. https://doi.org/10.7150/thno.16615.

Liu, Y., Haas, D.L., Poore, S., Isakovic, S., Gahan, M., Mahalingam, S., Fu, Z.F., Tripp, R.A., 2009. Human metapneumovirus establishes persistent infection in the lungs of mice and is reactivated by glucocorticoid treatment. J. Virol. 83, 6837–6848. https://doi.org/10.1128/JVI.00379-09.

Lorenz, W.W., Cormier, M.J., O'Kane, D.J., Hua, D., Escher, A.A., Szalay, A.A., 1996. Expression of the Renilla reniformis luciferase gene in mammalian cells. J. Biolumin. Chemilumin. 11, 31–37. https://doi.org/10.1002/(SICI)1099-1271. 199601)11:1 < 31::AID-BIO398 > 3.0.CO;2-M.

Luker, G.D., Luker, K.E., 2008. Optical imaging: current applications and future directions. J. Nucl. Med. 49, 1–4. https://doi.org/10.2967/jnumed.107.045799.

Matthews, J.C., Hori, K., Cormier, M.J., 1977. Substrate and substrate analogue binding properties of Renilla luciferase. Biochemistry 16, 5217–5220. https://doi.org/10.1021/bi00643a009.

McGavern, D.B., Kang, S.S., 2011. Illuminating viral infections in the nervous system. Nat. Rev. Immunol. 11, 318–329. https://doi.org/10.1038/nri2971.

McIntosh, K., Becker, W.B., Chanock, R.M., 1967. Growth in suckling-mouse brain of "IBV-like" viruses from patients with upper respiratory tract disease. Proc. Natl. Acad. Sci. U. S. A. 58, 2268–2273. https://doi.org/10.1073/pnas.58.6.2268.

Milne-Price, S., Miazgowicz, K.L., Munster, V.J., 2014. The emergence of the Middle East respiratory syndrome coronavirus. Pathog. Dis. 71, 121–136. https://doi.org/10.1111/2049-632X.12166.

Morfopoulou, S., Brown, J.R., Davies, E.G., Anderson, G., Virasami, A., Qasim, W., Chong, W.K., Hubank, M., Plagnol, V., Desforges, M., Jacques, T.S., Talbot, P.J., Breuer, J., 2016. Human coronavirus OC43 associated with fatal encephalitis. N. Engl. J. Med. 375, 497–498. https://doi.org/10.1056/NEJMc1509458.

Netland, J., Meyerholz, D.K., Moore, S., Cassell, M., Perlman, S., 2008. Severe acute respiratory syndrome coronavirus infection causes neuronal death in the absence of encephalitis in mice transgenic for human ACE2. J. Virol. 82, 7264–7275. https://doi.org/10.1128/JVI.00737-08.

Niu, P., Shen, J., Zhu, N., Lu, R., Tan, W., 2016. Two-tube multiplex real-time reverse transcription PCR to detect six human coronaviruses. Virol. Sin. 31, 85–88. https://doi.org/10.1007/s12250-015-3653-9.

Noah, B., Lecia, P., Kathryn, T., Stanley, P., 2006. Murine encephalitis caused by HCoV-OC43, a human coronavirus with broad species specificity, is partly immune-mediated. Virology 347, 410–421.

Perlman, S., Netland, J., 2009. Coronaviruses post-SARS: update on replication and pathogenesis. Nat. Rev. Microbiol. 7, 439–450. https://doi.org/10.1038/nrmicro2147.

Pichler, A., Prior, J.L., Piwnica-Worms, D., 2004. Imaging reversal of multidrug resistance in living mice with bioluminescence: MDR1 P-glycoprotein transports coelenterazine. Proc. Natl. Acad. Sci. U. S. A. 101, 1702–1707. https://doi.org/10.1073/pnas.0304326101.

Raaben, M., Prins, H.J., Martens, A.C., Rottier, P.J., De Haan, C.A., 2009. Non-invasive imaging of mouse hepatitis coronavirus infection reveals determinants of viral replication and spread in vivo. Cell Microbiol. 11, 825–841. https://doi.org/10.1111/j.1462-5822.2009.01298.x.

Rameix-Welti, M.A., Le Goffic, R., Herve, P.L., Sourimant, J., Remot, A., Riffault, S., Yu, Q., Galloux, M., Gault, E., Eleouet, J.F., 2014. Visualizing the replication of respiratory syncytial virus in cells and in living mice. Nat. Commun. 5, 5104. https://doi.org/10.1038/ncomms6104.

Reed, L.J., 1938. A simple method for estimating fifty percent endpoints. Am. J. Hyg. 37.

Savarino, A., Boelaert, J.R., Cassone, A., Majori, G., Cauda, R., 2003. Antiviral effects of chloroquine Effects of chloroquine on viral infections : an old drug against today ' s diseases ?.

Shen, L., Yang, Y., Ye, F., Liu, G., Desforges, M., Talbot, P.J., Tan, W., 2016. Safe and sensitive antiviral screening platform based on recombinant human coronavirus OC43 expressing the luciferase reporter gene. Antimicrob. Agents Chemother. 60, 5492–5503. https://doi.org/10.1128/AAC.00814-16.

St-Jean, J.R., Jacomy, H., Desforges, M., Vabret, A., Freymuth, F., Talbot, P.J., 2004. Human respiratory coronavirus OC43: genetic stability and neuroinvasion. J. Virol. 78, 8824–8834. https://doi.org/10.1128/JVI.78.16.8824-8834.2004.

Swanson 2nd, P.A., McGavern, D.B., 2015. Viral diseases of the central nervous system. Curr. Opin. Virol. 11, 44–54. https://doi.org/10.1016/j.coviro.2014.12.009.

Tannous, B.A., Kim, D.E., Fernandez, J.L., Weissleder, R., Breakefield, X.O., 2005. Codon-optimized Gaussia luciferase cDNA for mammalian gene expression in culture and in vivo. Mol. Ther. 11, 435–443. https://doi.org/10.1016/j.ymthe.2004.10.016.

Tregoning, J.S., Schwarze, J., 2010. Respiratory viral infections in infants: causes, clinical symptoms, virology, and immunology. Clin. Microbiol. Rev. 23, 74–98. https://doi.org/10.1128/CMR.00032-09.

van Boheemen, S., de Graaf, M., Lauber, C., Bestebroer, T.M., Raj, V.S., Zaki, A.M., Osterhaus, A.D., Haagmans, B.L., Gorbalenya, A.E., Snijder, E.J., Fouchier, R.A., 2012. Genomic characterization of a newly discovered coronavirus associated with acute respiratory distress syndrome in humans. mBio 3. https://doi.org/10.1128/mBio.00473-12.

van der Hoek, L., Pyrc, K., Jebbink, M.F., Vermeulen-Oost, W., Berkhout, R.J., Wolthers, K.C., Wertheim-van Dillen, P.M., Kaandorp, J., Spaargaren, J., Berkhout, B., 2004. Identification of a new human coronavirus. Nat. Med. 10, 368–373. https://doi.org/10.1038/nm1024.

Venisnik, K.M., Olafsen, T., Gambhir, S.S., Wu, A.M., 2007. Fusion of Gaussia luciferase to an engineered anti-carcinoembryonic antigen (CEA) antibody for in vivo optical imaging. Mol. Imaging Biol. 9, 267–277. https://doi.org/10.1007/s11307-007-0101-8.

Wilde De, A.H., Dirk, J., Posthuma, C.C., Zevenhoven-Dobbe, J.C., Stefan, V.N., Bestebroer, T.M., Hoogen Van Den, B.G., Johan, N., Snijder, E.J., 2014. Screening of an FDA-approved compound library identifies four small-molecule inhibitors of Middle East respiratory syndrome coronavirus replication in cell culture. Antimicrob. Agents Chemother. 58, 4875.

Woo, P.C., Huang, Y., Lau, S.K., Yuen, K.Y., 2010. Coronavirus genomics and bioinformatics analysis. Viruses 2, 1804–1820. https://doi.org/10.3390/v2081803.

Woo, P.C., Lau, S.K., Chu, C.M., Chan, K.H., Tsoi, H.W., Huang, Y., Wong, B.H., Poon, R.W., Cai, J.J., Luk, W.K., Poon, L.L., Wong, S.S., Guan, Y., Peiris, J.S., Yuen, K.Y., 2005a. Characterization and complete genome sequence of a novel coronavirus, coronavirus HKU1, from patients with pneumonia. J. Virol. 79, 884–895. https://doi.org/10.1128/JVI.79.2.884-895.2005.

Woo, P.C., Lau, S.K., Tsoi, H.W., Huang, Y., Poon, R.W., Chu, C.M., Lee, R.A., Luk, W.K., Wong, G.K., Wong, B.H., Cheng, V.C., Tang, B.S., Wu, A.K., Yung, R.W., Chen, H., Guan, Y., Chan, K.H., Yuen, K.Y., 2005b. Clinical and molecular epidemiological features of coronavirus HKU1-associated community-acquired pneumonia. J. Infect. Dis. 192, 1898–1907. https://doi.org/10.1086/497151.

Yiwu, Y., Zhen, Z., Yang, S., Xiao, L., Kai-Feng, X., Yuquan, W., Ningyi, J., Chengyu, J., 2013. Anti-malaria drug chloroquine is highly effective in treating avian influenza A H5N1 virus infection in an animal model. Cell Res. 23, 300–302.

Yu, J.E., Kim, M., Lee, J.H., Chang, B.J., Song, C.S., Nahm, S.S., 2014. Neonatal influenza infection causes pathological changes in the mouse brain. Vet. Res. 45, 63. https://doi.org/10.1186/1297-9716-45-63.